CLIMATOLOGY

The internal origin of the west-east asymmetry of Antarctic climate change

Sang-Yoon Jun[1]*, Joo-Hong Kim[1]*, Jung Choi[2], Seong-Joong Kim[1†], Baek-Min Kim[3], Soon-Il An[4]

Recent Antarctic surface climate change has been characterized by greater warming trends in West Antarctica than in East Antarctica. Although this asymmetric feature is well recognized, its origin remains poorly understood. Here, by analyzing observation data and multimodel results, we show that a west-east asymmetric internal mode amplified in austral winter originates from the harmony of the atmosphere-ocean coupled feedback off West Antarctica and the Antarctic terrain. The warmer ocean temperature over the West Antarctic sector has positive feedback, with an anomalous upper-tropospheric anticyclonic circulation response centered over West Antarctica, in which the strength of the feedback is controlled by the Antarctic topographic layout and the annual cycle. The current west-east asymmetry of Antarctic surface climate change is undoubtedly of natural origin because no external factors (e.g., orbital or anthropogenic factors) contribute to the asymmetric mode.

INTRODUCTION

Climatic warming over Antarctica has been a matter of grave consequence because even partial ice sheet collapse would have substantial impacts on hemispheric climate through freshwater discharge into the Southern Ocean (*1*, *2*) and global climate through rising of the sea level (*1*). Half-century reconstructed Antarctic surface air temperature (SAT) data have revealed differing strengths and seasonalities in warming trends depending on subcontinental regions (*3*–*8*). Various local and remote factors have been suggested to explain the season-dependent spatially inhomogeneous trends (*7*, *9*–*13*). Positive trends in the Southern Annular Mode (SAM) (*14*) in austral summer and autumn, which are attributed to stratospheric ozone depletion and increase in carbon dioxide (*9*, *10*, *12*, *15*), are the most well-known factors explaining cooling over the ice sheet and warming over the Antarctic Peninsula (AP). However, explanations based on the positive SAM trend in austral summer and autumn have a limitation in clearly accounting for the broader rapid warming trend over West Antarctica [i.e., the AP toward the West Antarctic Ice Sheet (WAIS)] in austral winter and spring and weak all-season warming over the East Antarctic Ice Sheet (EAIS), which has been suggested by reconstructed datasets (*5*, *7*, *12*).

To resolve this limitation, new mechanisms relying on the atmospheric Rossby wave bridge from sea surface temperature (SST) forcing over the lower latitudes toward the West Antarctic sector have been proposed (*7*, *11*, *16*). However, these explanations do not fully account for amplified warming over the entire West Antarctica, the outstanding pattern of the half-century trend (*13*, *17*). The warming of tropical Atlantic SSTs was proposed as a factor to warm the AP in austral winter by strengthening the Amundsen Sea Low (ASL) (*16*). However, the tropical–West Antarctic connection is not readily applicable to explaining the trend because the teleconnection is derived at the subdecadal time scale after removing the linear trend, and in austral winter, there has been neither a strengthening trend in the ASL (*18*) nor a trend in the dominant Rossby wave pattern [i.e., the Pacific–South American (PSA) pattern (*19*)] consistent with observed warming over West Antarctica (*17*).

Because of the abundant efforts given toward observation, reconstruction, and numerical modeling, uncertainties in the formation of spatial patterns and seasonalities in Antarctic climate change have been considerably resolved over the last two decades. However, this issue remains a daunting challenge because of its fundamental linkage with the multidecadal natural variability in the coupled ocean-atmosphere climate system. There are inherent difficulties in understanding multidecadal time scales arising from insufficient modern instrumental records, uncertainties in the reconstructed proxy records, and imperfect numerical models.

Although multiple mechanisms, including both forced and natural origins, contribute to the west-east asymmetry of Antarctic climate change in complicated ways, this pattern should primarily be manifested through internal factors within Antarctica. On the basis of this idea, we aim to prove that the asymmetry of the temperature trend comes from the robust high-latitude mode of multidecadal natural variability, inducing inverse temperature anomalies between the two subcontinents that internally originate in and around Antarctica. Here, "internal origin" implies that the phenomenon originates primarily from high latitudes, combined with WAIS-EAIS topographical distinction and winter amplification of the atmospheric dynamical response to multidecadal SST variability in the Amundsen-Bellingshausen seas (ABS) (*20*–*22*).

RESULTS

Recent climate change in Antarctica

Figure 1A shows the trends in annual-mean Antarctic SATs during 1958–2012 from the reconstructed data (NB2014) (*12*), with the trends in the annual-mean SSTs over the surrounding ocean from the Hadley Centre sea ice and SST dataset version 1 (HadISST1) (*23*). The stronger warming trends prevail over West Antarctica, mainly contributing to the continental average warming trend (Fig. 1D) (*5*). The SAT trend pattern suggests the possibility of decomposing a physical climate mode concerning amplified warming over West Antarctica. Thus, we apply the empirical orthogonal function (EOF) analysis to annual-mean SATs over Antarctica, which yields the first EOF mode (EOF1) representing single-signed variability

[1]Korea Polar Research Institute, Incheon, South Korea. [2]Seoul National University, Seoul, South Korea. [3]Pukyong National University, Busan, South Korea. [4]Yonsei University, Seoul, South Korea.
*These authors contributed equally to this work.
†Corresponding author. Email: seongjkim@kopri.re.kr

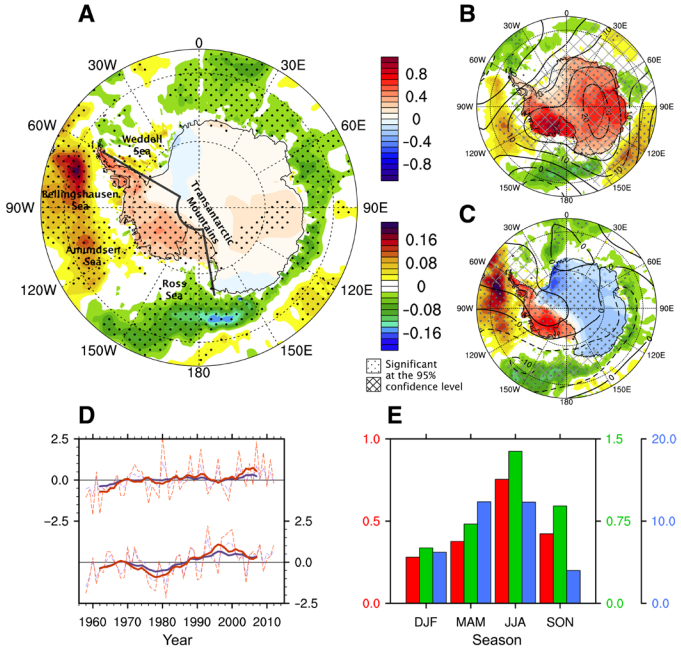

Fig. 1. Annual-mean trend and two leading modes of Antarctic surface temperature during 1958 to 2012. (**A**) Trends in the SAT (in K decade^{-1}) and SST (in K decade^{-1}) and (**B** and **C**) the two leading EOFs of the annual-mean SAT during 1958 to 2012 and its regressed SAT (in K, shading over Antarctica), 300-hPa geopotential height (in meters, contour), and SST (in K, shading over the ocean). The dark gray line in (A) indicates the dividing boundary for East and West Antarctica. (**D**) Year-to-year variations in the average over all of Antarctica (in K, red line), the corresponding PC of EOF1 (unitless, blue line) (top), the difference between West and East Antarctica (in K, red line), and the corresponding PC of EOF2 (unitless, blue line) (bottom). The thick lines indicate 10-year running means. (**E**) Seasonal characteristics of the second EOF PC: correlation coefficients with the second EOF PC of seasonal mean SAT (unitless, red bar), the difference between West and East Antarctica in regressed seasonal mean SAT (in K, green bar), and area-averaged heights over the 60°S to 85°S, 150°W to 50°W in regressed seasonal mean 300-hPa geopotential height (in meters, blue bar).

over the entire continent (Fig. 1B) and the second EOF mode (EOF2) representing a seesaw pattern with its node along the Transantarctic Mountains (TAM) (Fig. 1C). The leading two EOF modes are nondegenerate by the calculation of sampling error estimates (see fig. S1) (*24*). It is noted that these patterns are slightly different from those of the monthly satellite-derived surface temperatures during 1982–1999 (*25*), in which EOF2 had smaller explained variances and EOF1 had larger EOF loadings over the EAIS. The EOF sensitivity tests indicate that the difference between our case and a previous work by Schneider *et al.* (*25*) mainly originates from the input data but not from the temporal resolutions of the input time series (e.g., annual-mean, seasonal-mean, or monthly-mean time series) or from the start and end years of the time series (see Materials and Methods and figs. S2 to S5). In addition, the same signed variation over both the AP and WAIS in the EOF2 occurs only during the long-term period but not in the short-term period, regardless of the temporal resolution. This suggests that there may exist same-signed low-frequency variability over the AP and WAIS. Corresponding principal components (PCs) present common increasing trends, but the EOF2 PC has more pronounced multidecadal fluctuations embedded in the trend (Fig. 1D). In the concurrent positive phase of the two modes, West Antarctica experiences substantial warming by the reinforcement of the two modes, while over East Antarctica, opposite-signed variabilities in the two modes lead to weak warming.

The SST trends for the same period show a zonal asymmetry in their signs between the ABS sector and the surrounding Antarctic seas (Fig. 1A). Although few observations over the Southern Ocean result in large uncertainties in the SST data, the overall pattern of the SST trends surrounding Antarctica is reasonable based not only on the previous analyses on the trends in Southern Ocean SSTs and sea ice cover since 1979 (*26*) but also on the estimates from the HadSST3 observations (*27*). While warming over the ABS sector has paused since the early 2000s (*28*), the area-averaged cooling over the rest of the surrounding seas has continued during the analysis period from 1958 to 2012 (fig. S6). It is noted that the slowdown in the SST warming trend over the ABS sector concurrently occurred with that in the increasing trend in the indices of the EOF2 PC and west-east SAT difference. This indicates the critical role of atmosphere-ocean coupling over the ABS sector in forming the EOF2 PC of Antarctic SATs.

The regressed patterns of SSTs and 300-hPa geopotential heights corresponding to the two EOFs show that EOF1 is associated with the single-signed change in Antarctic air masses and the wavy SST change from the outer Weddell Sea sector to the Southeast Indian Ocean sector through the Amundsen-Ross seas (Fig. 1B), forming a wave number 3 structure that is one of the prominent features of the Southern Hemisphere extratropical circulation (*29*, *30*). By contrast, EOF2 presents a similar pattern to that of the SST trends seen in Fig. 1A, with the dipolar redistribution of Antarctic air masses (Fig. 1C). The greater resemblance of the spatial trend pattern derived in EOF2 (Fig. 1C) to that of the trend (Fig. 1A) indicates its critical role in illustrating the recent Antarctic surface temperature trend. EOF1 can be interpreted as a SAM pattern mixed with a PSA-1 pattern. Individual correlations of the EOF1 PC with various climate indices, such as the SAM, PSA-1, PSA-2 (*19*), and three El Niño–Southern Oscillation (ENSO) indices (NINO3, NINO3.4, and NINO4), yield the largest coefficient for the SAM (−0.39), followed by that for the PSA-1 (−0.25) (Table 1). From the EOF sensitivity tests, the SAM and PSA together induce single-signed variability over most of Antarctica, resembling the regressed pattern of EOF1 (fig. S7). On the other hand, EOF2 has a trace of the PSA-2 in the regression pattern, with its PC having the best correlation with the PSA-2 index (−0.41) (Table 1). The linkage of EOF2 with the PSA-2, being maximized in austral winter, is more persistent for all seasons than those of EOF1 with the SAM or PSA-1, which was also recognized in the previous study (*25*). From the regression and correlation analyses, the west-east asymmetric mode in Antarctic SATs (Fig. 1A) is likely to be forced by asymmetric SST variability between the ABS sector and the rest of the seas surrounding Antarctica, which looks to be more relevant to the PSA-2–type high-latitude atmospheric variability.

Seasonality is key to understanding the mechanism behind Antarctic climate change (*7*, *13*). The EOF2 PC of annual-mean SATs shows the largest correlation with that of winter [June-July-August (JJA)] mean SATs (red bars in Fig. 1E). The west-east SAT difference (green bars in Fig. 1E) and the 300-hPa geopotential height averaged over the domain of 50°W to 150°W, south of 60°S (blue bars in Fig. 1E) are also largest in EOF2 of the winter mean SATs. While the largest warming over West Antarctica since 1958 occurred in

Table 1. Correlation coefficients of the two leading modes with climate indices. Correlation coefficients of the two leading modes of annual-mean surface temperature with the following climate indices: SAM, Pacific South America (PSA)–1, PSA-2, NINO3, NINO3.4, and NINO4. The bold values indicate that the correlation coefficient is significant at the 99% confidence level. For the Student's *t* test, we reduced the number of degrees of freedom by using the effective sample size.

	EOF1 (ANN)	EOF2 (ANN)	EOF1 (DJF)	EOF2 (DJF)	EOF1 (MAM)	EOF2 (MAM)	EOF1 (JJA)	EOF2 (JJA)	EOF1 (SON)	EOF2 (SON)
SAM	**−0.39**	0.16	**−0.49**	0.11	**−0.66**	−0.13	**−0.67**	0.08	−0.29	0.18
PSA-1	−0.25	−0.25	**−0.44**	0.03	−0.17	−0.14	−0.19	−0.17	**−0.49**	0.09
PSA-2	0.10	**−0.41**	**0.43**	−0.26	−0.04	**−0.46**	0.01	**−0.47**	−0.17	**−0.36**
NINO3	−0.15	−0.07	0.17	−0.09	0.02	−0.03	−0.03	−0.03	−0.12	0.12
NINO3.4	−0.11	−0.17	0.19	−0.11	0.08	−0.09	0.03	−0.05	−0.15	0.09
NINO4	0.21	−0.20	0.26	0.00	0.11	−0.13	0.18	−0.11	−0.03	−0.05

austral spring (*7*, *12*, *13*), warming over West Antarctica and cooling over East Antarctica are apparent in JJA (*12*). The EOF2 spatial pattern also amplifies in winter (fig. S2). Thus, it is concluded that EOF2 is the mode that is amplified in austral winter, forming the west-east SAT asymmetry in Antarctic climate change. This is partly illustrated on the basis of the statistics that the PSA-2 type is most frequently observed in winter (*31*).

Representation in climate models

Modern instrumental records over Antarctica are too short to illustrate the potential multidecadal natural variability in these climate modes. Furthermore, the single observational representation limits our confidence in elucidating the nature of the variability. Therefore, climate model simulations are valuable for complementing observational deficiencies over Antarctica. Thus, we examine the widely used multimodel data from the Coupled Model Intercomparison Project phase 5 (CMIP5) (*32*). A common basis function (CBF) analysis, which is a useful tool to reveal the observed mode in the model world (*33*), also reveals the two leading modes in the historical simulations of 38 CMIP5 models for the same period of 1958–2012 (Fig. 2, A and B). Most CMIP5 models simulate two observed modes with amplitudes of more than 0.8 (Fig. 2C). The marks near the amplitude with a value of 1 on the *x* axis indicate that the models simulate the observed variability with almost the same intensity in the variance of the PC time series. In addition, the physical and seasonal characteristics of the leading modes are well simulated by the CMIP5 models. Relationships of the leading modes with SSTs and 300-hPa geopotential heights are consistently found in their regressed patterns, including the zonally wavy SST relationship in the first mode (Fig. 2, A and B). The seasonality of the second mode in surface asymmetry is also found in the CMIP5 multimodel mean values (Fig. 2D).

This consistency of the two climatic modes in the CMIP5 models, as in NB2014, suggests the robustness of these modes in accounting for the change in Antarctic SATs. The first mode robustly shows an increasing trend in the CMIP5 models, as it does in the observations (see the red circles in Fig. 2C). The strengthening of the first mode under global warming in NB2014 and the CMIP5 historical simulations suggests that this mode might be closely linked to a global temperature rise. This can also be inferred from the substantial across-model correlation between the simulated global mean temperature trend and the amplitude of the first mode

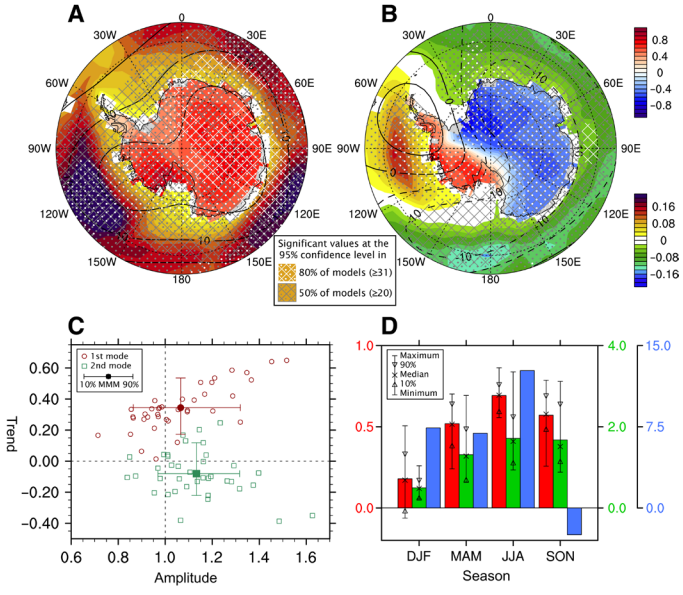

Fig. 2. Two leading modes of the annual-mean Antarctic surface temperature and their characteristics during 1958 to 2012 in the CMIP5 historical simulations. (**A** and **B**) Multimodel mean (MMM) regression pattern of annual-mean SAT (in K), SST (in K), and 300-hPa geopotential height (in meters) in the 38 CMIP5 models for the (A) first and (B) second EOF modes of NB2014 by CBF analysis. (**C**) Scatterplot of the amplitudes and trends (in K decade^{-1}) of the PC time series from the CMIP5 models normalized by the SD of the NB2014. The amplitudes are defined by the ratio of the CMIP5 model to the NB2014. (**D**) MMM characteristics of the second EOF mode of Antarctic SAT during each season: correlation coefficients of the second EOF PC of seasonal mean SAT with annual-mean SAT (unitless, red bar), the difference between West and East Antarctica in regressed seasonal mean SAT (in K, green bar), and area-averaged heights over the 60°S to 85°S, 150°W to 50°W in regressed seasonal mean 300-hPa geopotential height (in meters, blue bar). Whisker lines for the blue bar are not shown according to their large range.

in the CMIP5 models (r = 0.61). However, the second mode shows a weak negative trend in multimodel mean values in contrast to the increasing trend in the observations. Discrepancies in the second mode might be one of the reasons why the CMIP5 models could not capture recent Antarctic asymmetric trends (*13*).

To find robust evidence for the characteristics of the two modes in the longer period, we further analyze multiple datasets of long-term Antarctic surface temperatures, including proxy-based reconstruction

data and climate modeling results: surface temperature reconstruction for the last 2000 years (PAGES Antarctica2k) (*34*), two long-term modeling results from the mid-Holocene [LOVECLIM and TraCE-21K (*35*)], and four simulations for the 20th and 21st centuries by CESM1 (see Materials and Methods). Despite the diversity of data sources, all datasets consistently show the first mode explaining the same change across the entire Antarctic and the second mode presenting the asymmetric change over Antarctica in the EOFs of Antarctic surface temperatures (Fig. 3). The spectra analysis shows that second PCs have interannual variabilities in all datasets and multidecadal variabilities in datasets longer than 1000 years.

In addition, the first PCs from all datasets reflect the long-term variation in radiatively forced global-scale climate change: a gradual cooling from the mid-Holocene to the present (LOVECLIM); an abrupt warming after a long-term cooling trend, shaped similarly to a hockey stick, during the last two millennia (PAGES Antarctica2k); and a sustained warming in the historical and future simulations under greenhouse gas (GHG) influences by CESM1-CAM5 (Fig. 4A). In contrast, all of the second PCs do not display any secular trends reflecting global-scale climate change (Fig. 4B). Comparing the CESM1 simulations under different global-scale forcings verifies the role of leading modes in Antarctic surface change (Fig. 4A). In the historical simulation without GHG forcing, the first PC has no long-term trend. The 20th century historical simulation under GHG forcing and the 21st century simulations with the RCP4.5 and RCP8.5 scenarios, however, consistently show an increasing trend in the first PC. Another noticeable feature in future scenario runs is the increases in the explained variance of EOF1 as global warming intensifies, indicating that increasing surface temperatures across Antarctica might dominate over the west-east asymmetric temperature change (Fig. 3). In all of these simulations, the second PC has no long-term trend (Fig. 4B), which is consistent with previous results, and its explained variance decreases with the increase in GHG forcing (Fig. 3). That is, all of these results strongly suggest that the first mode is closely linked to global-scale climate change, while the second mode might be associated with the internal variability within the Antarctic environment.

Self-sustained asymmetric Antarctic climate variability

The fact that the second mode consistently shows no relationship with external global-scale forcing changes in the diverse datasets suggests that this variability could be manifested by climate factors in the Antarctic and adjacent regions. The Antarctic topographical

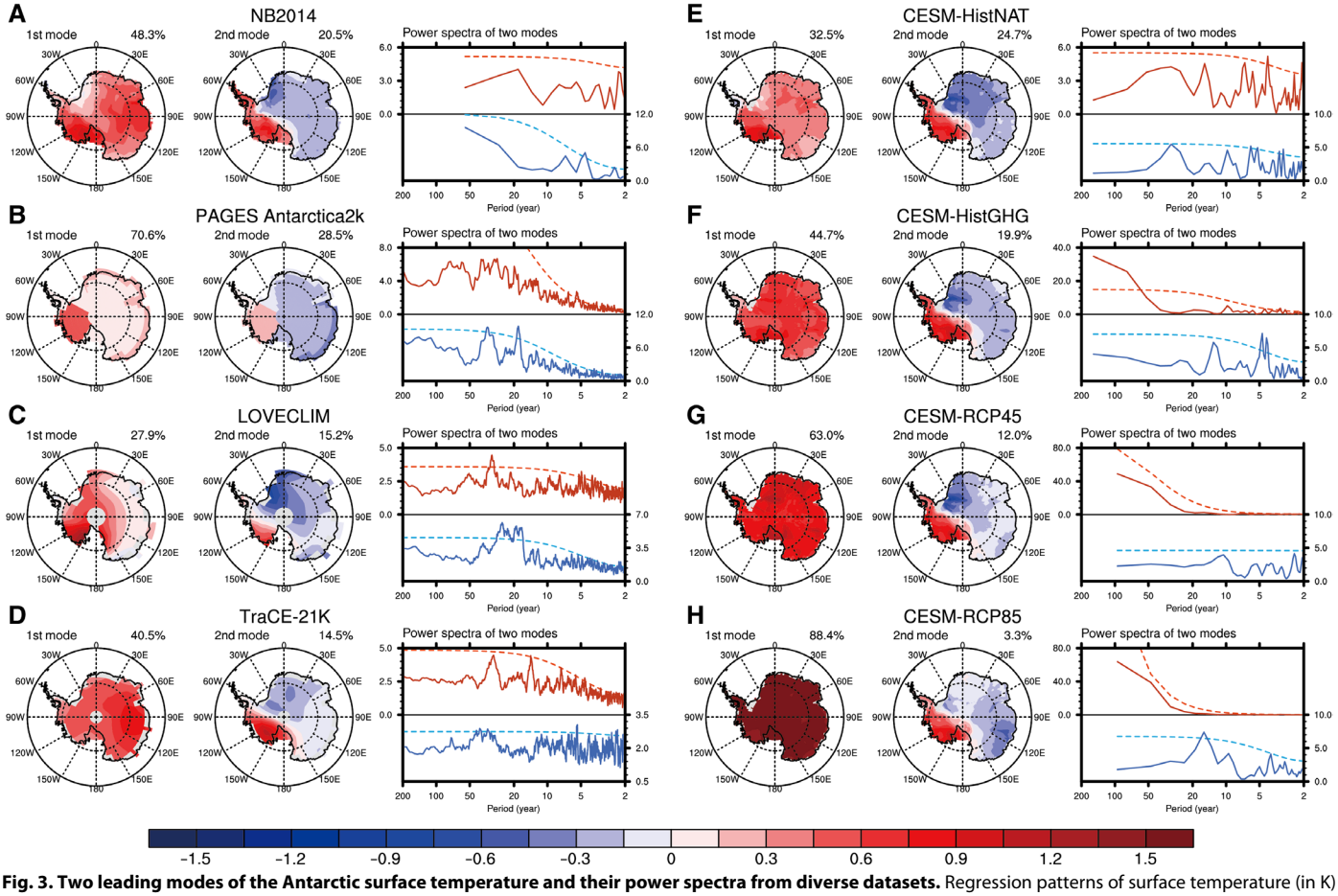

Fig. 3. Two leading modes of the Antarctic surface temperature and their power spectra from diverse datasets. Regression patterns of surface temperature (in K) for the first and second EOFs, and power spectra of their corresponding PCs from the (**A**) NB2014, (**B**) PAGES Antarctica2k, (**C**) LOVECLIM, (**D**) TraCE-21K, and 4 CESM simulations under the CMIP5 scenarios: (**E**) historical natural forcing only, (**F**) historical greenhouse gases forcing, (**G**) RCP4.5, and (**H**) RCP8.5. The red and blue solid lines indicate the spectra of the first and second EOFs, respectively. Dashed lines indicate the significant limits at the 95% confidence level. The explained variance in the EOF mode is written in the upper-right corner of each EOF mode.

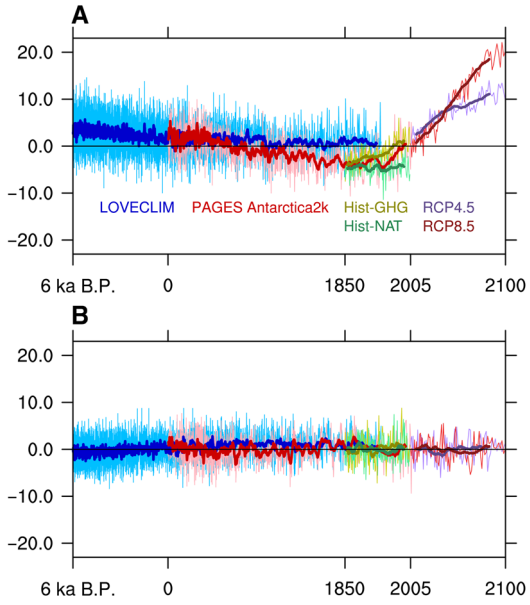

Fig. 4. Temporal evolution of the two leading modes in various datasets covering the last 6000 years. PCs of the (**A**) first and (**B**) second EOFs for annual-mean surface temperature from the LOVECLIM (blue), PAGES Antarctica2k (red), CESM1 historical-GHG (yellow green), CESM1 historical-NAT (green), CESM1 RCP4.5 (purple), and CESM1 RCP8.5 (dark red) datasets. The thick lines indicate the 20-year running mean of each PC. All PCs are rescaled with the SD of the PC from LOVECLIM.

distinction between the WAIS and EAIS, divided by the TAM, could be a major factor because it differentiates any influence on Antarctica between the two ice sheets. Thus, we perform sensitivity experiments on changing Antarctic terrains using a coupled atmosphere-ocean model to demonstrate whether the topographical distinction is a key factor behind the asymmetric climate mode. With the current Antarctic terrain, the coupled atmosphere-ocean model produces an asymmetric mode similar to that observed in terms of the spatial pattern (Fig. 5A). The experiment with the flattened EAIS shows that the asymmetric mode becomes stronger with the expansion of the West Antarctic warm region farther toward East Antarctica (Fig. 5B). In contrast, the elevated WAIS experiment produces a weak asymmetry with the negligible West Antarctic warming (Fig. 5C).

From these experiments, we can deduce the role of the Antarctic topographic layout in controlling the tropospheric circulation and consequent SAT variation over Antarctica. The current lower West Antarctic terrain allows warm air to be advected from the Amundsen-Ross seas to West Antarctica, while the steep TAM hinders warm air from flowing toward East Antarctica. Across the heated West Antarctic coastal region, the barotropic anticyclone system develops, which can reinforce warm advection from the Amundsen-Ross seas (Fig. 5, D and E). The heat transport by synoptic eddy activity over the west Antarctic coastal region contributes to reinforcement in warm air advection (*36*), and the contribution of synoptic eddy activity could increase under the flattened Antarctic topography (*37*). In addition, the anticyclone system also enforces southward meridional oceanic flow over the ABS by Ekman transport, which supplies warm water from the extratropics to these seas (Fig. 5, G and H). Eventually, the warmer land surface, the development of the anticyclone system, and the warmer ocean surface together strengthen the warming over West Antarctica by promoting each other. The mutual cooperation of these factors can be confirmed in the two altered terrain experiments. The absence of the TAM preferentially enforces warm advection to the central Antarctic and, in turn, strengthens the asymmetry by promoting all of these contributing factors (Fig. 5, B, E, and H). In contrast, the higher WAIS preferentially prevents warm advection from the adjacent ocean and consequentially weakens the asymmetry by breaking the mutual cooperation (Fig. 5, C, F, and I). That is, the harmony of the atmosphere-ocean coupled feedback over the ABS and the Antarctic terrain can induce the west-east asymmetric natural variability in Antarctic surface temperature. The formation of the anticyclonic system over the coastal ABS region by the mutual processes seems to be a key factor to explain seasonality because the polar barotropic anticyclone system can be developed by surface warming more dominantly during cold seasons (*38*, *39*).

To isolate the individual roles of the tropical Pacific (15°S to 15°N, 150°E to 60°W) and the West Antarctic Ocean (55°S to 90°S, 150°E to 60°W) on the Antarctic climate asymmetry, we conduct additional atmospheric model experiments by prescribing SSTs obtained from the coupled model experiment (fig. S8A). The experiment with isolated tropical Pacific SST forcing shows a prominent teleconnection response of geopotential heights toward Antarctica with a wintertime SAT warming response over East Antarctica as well as West Antarctica (fig. S8, B to F). The experiment with isolated West Antarctic SST forcing also displays an apparent winter-maximized asymmetric temperature response, even though the response of geopotential height is relatively weaker (fig. S8, G to K). These results lead us to conclude that (i) the tropical forcing contributes more to the response of the upper-tropospheric anticyclonic circulation, and (ii) the Antarctic near-surface west-east asymmetric pattern is better represented by the regional West Antarctic SST forcing. However, it should be noted that neither can be regarded as "proven" without question because the atmospheric model lacks the role of atmosphere-ocean coupled interaction. Therefore, an additional coupled model sensitivity experiment, in which the tropical Pacific is partially prescribed with climatological SSTs, is needed for the comparison with the baseline coupled model experiment. This is beyond the scope of this study.

DISCUSSION

The model experiments conducted by CESM1 were not enough to fully confirm the roles of different regional SST forcings. Thus, we try to reinforce our logic weighted to the local atmosphere-ocean coupled feedback off West Antarctica through inference by comparing the regressed SST patterns among HadISST1, 38 CMIP5 models (CMIP5 MMM), and CESM1 onto their respective normalized EOF2 PC time series (fig. S9). In the tropics, there are large discrepancies between the observation and models, i.e., tropical central Pacific cooling in HadISST1, overall tropical and midlatitude cooling in CMIP5 MMM, and El Niño in CESM1. The large discrepancy in the tropical pattern associated with the Antarctic asymmetric mode implies that the dominant contribution of the tropical SST forcing to the upper-tropospheric anticyclonic circulation over West Antarctica cannot be generalized. By contrast, the consistent pattern of the warmer ABS SST is seen over the Southern Hemisphere high-latitude ocean. On the basis of this fact, it is natural to determine that the regional SST anomalies around Antarctica

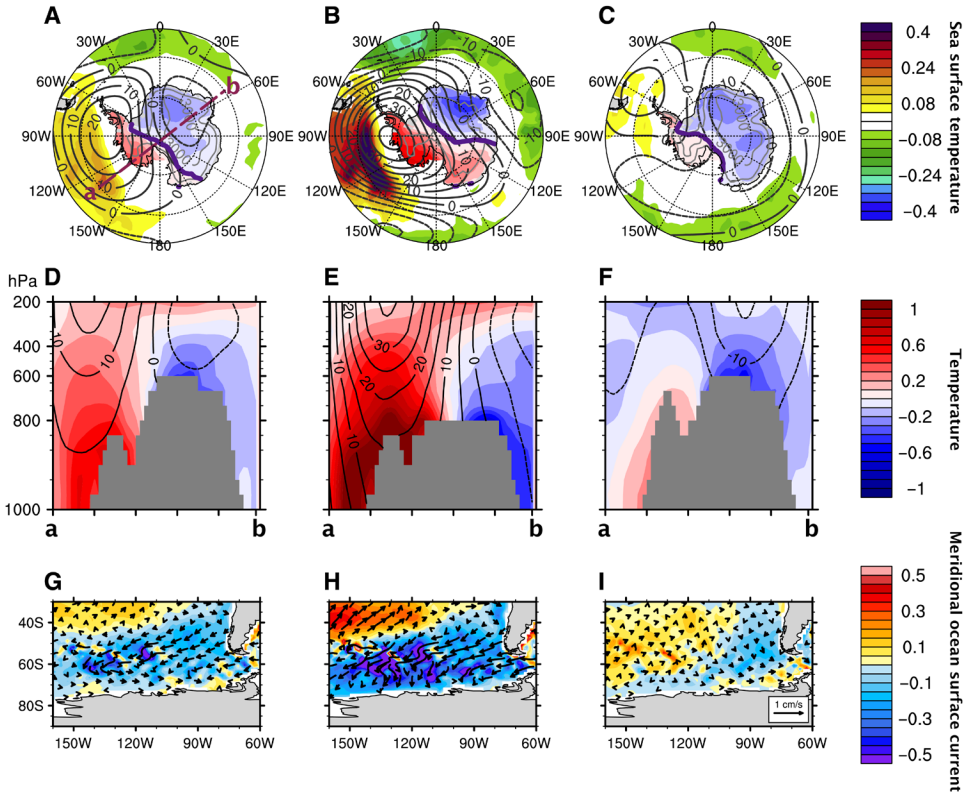

Fig. 5. West-East Antarctic asymmetric modes according to the Antarctic terrain. Regressions of the annual-mean surface temperature onto the EOF mode representing the east-west Antarctic asymmetry from coupled atmosphere-ocean model experiments with three different Antarctic terrains: (**A, D,** and **G**) current Antarctic terrain, (**B**, **E**, and **H**) East Antarctic terrain lowered to 1500 m, and (**C**, **F**, and **I**) West Antarctic terrain elevated with a factor of 2. The explained variances in these asymmetric modes are 19.6, 33.0, and 20.7%, respectively. Shading over the Antarctic continent, shading over the ocean, and the black contour lines in the top panels indicate the regression patterns of the annual-mean SAT (in K), SST (in K), and 300-hPa geopotential height (in meters), respectively. The thick gray contour line over the Antarctic continent indicates the elevation of the terrain. Shading and contour lines in the middle panels indicate the regressions of air temperature (in K) and geopotential height (in meters) for each asymmetry mode along the great circle line from 160°W 60°S (a) to 55°E 60°S (b) [the dashed purple line on (A)], respectively. Vector and shading over the ocean in the bottom panels indicate the regressions of ocean surface current and its meridional component for each asymmetry mode, respectively.

are the essential component for the asymmetry. The consistency between the observation and models over the high-latitude ocean enables us to think it reasonable to argue the harmony of the atmosphere-ocean coupled feedback off West Antarctica and the Antarctic terrain to generate the Antarctic west-east asymmetric natural variability.

In the asymmetric mode of Antarctic SATs, multidecadal variability is found in the long paleoclimate datasets of PAGES Antarctica2k, LOVECLIM, and TraCE-21K. This suggests that the enhanced asymmetric trend between West and East Antarctica during recent decades could be a manifestation of multidecadal variability. The linkage between the climatic conditions over the ABS and the Antarctic surface asymmetry at different time scales seems to determine time scales with either interannual or multidecadal variabilities. First, because the atmospheric Rossby wave bridge makes the connection between the tropics and west Antarctic surface climate (*7*, *11*, *16*), strong interannual variability in the tropics, such as ENSO, might contribute to variability in the Antarctic asymmetric mode. On the other hand, different seasonalities in the interaction between the atmosphere and ocean could alter the interannual variability because the interaction between sea level pressure and surface temperature over the Bellingshausen Sea has strong seasonality. Their correlation coefficients shift from negative during austral summer ($r = -0.17$ for February) to positive during austral winter ($r = 0.53$ for August). This seasonality contributes to the wintertime development of the asymmetric mode, including the increase in surface temperature and the high-pressure system over this region, but disturbs the persistence of asymmetry in the following warm season. Second, the long-term variability in the ocean over the West Antarctic coastal region seems to play a role in producing multidecadal periodicity. There have been some reports on long-term variability of the ocean in this region via ocean circulation changes (*20*, *21*, *26*). Possible roles of the ocean through the ASL have been suggested (*20*), but the relationship between the ocean and ASL is not immediately clear.

The climatic modes in this study suggest an important implication for future climate change in East Antarctica under global warming. The two future climate change experiments suggest that the explained variance in the first mode is much higher in the 21st century, while the second mode diminishes. The characteristics of the two modes strongly suggest that if global warming continues, a substantial temperature increase over East Antarctica may occur in addition to ongoing West Antarctic warming. The asymmetric mode will persist at its own pace in the future, even

under global warming, but its role may not be as great as it is now. The intensified global warming over all of Antarctica in the future can induce massive melting of the ice shelves, even in East Antarctica. This explains why we have to keep an eye on Antarctica as global warming continues, despite the recent mitigation of warming in the eastern part of the region, due to the asymmetric nature of climate change.

MATERIALS AND METHODS

Datasets

We used the monthly surface temperature data from 1958 to 2012 reconstructed by Nicolas and Bromwich (*12*). This dataset was reconstructed with a new temperature record from Byrd station (80°S 119.5°W) in the WAIS that was not included in the previous Antarctic surface temperature reconstructions. Therefore, this dataset might be more vital for presenting past temperature changes in West Antarctica than other reconstructions. For the last two millennia, PAGES-2K Antarctic surface temperature reconstruction based on ice-core proxies (PAGES Antarctica2k) (*34*) was conducted. The 300-hPa geopotential height field from JRA55 (*40*) and SST of the HadISST1 (*23*) and HadSST3 (*27*) datasets for the period of 1958–2012 were used.

Surface temperature, SST, and 300-hPa geopotential height in the historical and RCP4.5 simulations by the 38 CMIP5 models (*32*) were combined for the period of 1958–2012. The simulation results from 6 thousand years (ka) before present (B.P.) to 1 ka B.P. were extracted from TraCE-21K (*35*). In addition, the CESM1-CAM5 simulations under the historical-GHG, historical-NAT, RCP4.5, and RCP8.5 scenarios were used to compare the effect of global-scale radiative forcing on present and future climate.

Model experiments

We conducted two climate models in this study: LOVECLIM (*41*) and CESM1 (*42*). The LOVECLIM, the Earth system model of intermediate complexity, was used to produce climate change from 6 ka B.P. to 0 B.P. under changing orbital conditions. In the LOVECLIM experiment, we chose the atmosphere, ocean/sea-ice, and land component models. In addition, CESM version 1.2 was used for sensitivity experiments. Fully coupled settings (atmosphere, land, ocean, and sea ice) under preindustrial conditions were selected to examine the effect of Antarctic terrains with three different topographies. We performed simulations for 200 years with the current Antarctic topography and two additional topographies by flattening the East Antarctic region to 1500 m and by elevating the West Antarctic region with a factor of 2. We used the last 100 years of these results. In addition, atmosphere-only setting was applied to investigate the role of isolated SST anomalies over the tropical Pacific (15°S to 15°N, 150°E to 60°W) and the West Antarctic Ocean (55°S to 90°S, 150°E to 60°W) for the Antarctic climate asymmetry. For the experiments, the composite SST and sea ice anomalies were obtained from the fully coupled experiment by selecting cases of the large positive phase (above 1.5σ) of the Antarctic asymmetric mode (i.e., EOF2) (fig. S8A). In addition to the baseline experiment, where the climatological SST and sea ice from the coupled model experiment were prescribed, two sensitivity experiments respectively with composite SST anomalies of the tropical Pacific and the West Antarctic sector were performed. These atmosphere model simulations were integrated for 50 years.

The analysis for the leading modes of Antarctic surface temperature

We used EOF analysis to find the leading modes in Antarctic surface temperature. The EOF analysis was performed to surface temperature over the entire Antarctic continental area during the entire years of each dataset. The PAGES Antarctica2k dataset has different periods per grid point (e.g., region), so we chose the East Antarctic Plateau and WAIS regions, which can represent East and West Antarctica, respectively, and fully cover the last two millennia in this dataset.

To compare previous EOF analysis results based on different periods (1982–1999) and datasets (satellite-derived surface temperatures) (*25*), we performed EOF analysis with monthly, annual-mean, and seasonal-mean values from NB2014 for the two periods of 1958–2012 and 1982–1999 (figs. S1 to S4).

The CBF analysis was used to examine the leading modes for the Antarctic surface temperature in the historical simulations by the CMIP5 models (*33*). In the CBF analysis, the model anomalies were projected onto the observed EOF. In this study, we projected the two leading modes of annual-mean surface temperature from NB2014 to the modeled surface temperature anomalies for the same period as that of the observations (1958–2012), combined with the CMIP5 historical and RCP4.5 simulations. With this projection, we fetched the PCs of the two observed EOFs from the CMIP5 models. All datasets were interpolated to 2.5° by 2.5° before performing the CBF analysis.

SUPPLEMENTARY MATERIALS

Supplementary material for this article is available at http://advances.sciencemag.org/cgi/content/full/6/24/eaaz1490/DC1

REFERENCES AND NOTES

1. N. R. Golledge, E. D. Keller, N. Gomez, K. A. Naughten, J. Bernales, L. D. Trusel, T. L. Edwards, Global environmental consequences of twenty-first-century ice-sheet melt. *Nature* **566**, 65–72 (2019).
2. F. Schloesser, T. Friedrich, A. Timmermann, R. M. DeConto, D. Pollard, Antarctic iceberg impacts on future Southern Hemisphere climate. *Nat. Clim. Change* **9**, 672–677 (2019).
3. W. L. Chapman, J. E. Walsh, A synthesis of antarctic temperatures. *J. Climate* **20**, 4096–4117 (2007).
4. D. H. Bromwich, J. P. Nicolas, A. J. Monaghan, M. A. Lazzara, L. M. Keller, G. A. Weidner, A. B. Wilson, Central west antarctica among the most rapidly warming regions on earth. *Nat. Geosci.* **6**, 139–145 (2012).
5. E. J. Steig, D. P. Schneider, S. D. Rutherford, M. E. Mann, J. C. Comiso, D. T. Shindell, Warming of the antarctic ice-sheet surface since the 1957 international geophysical year. *Nature* **457**, 459–462 (2009).
6. R. O'Donnell, N. Lewis, S. McIntyre, J. Condon, Improved methods for PCA-based reconstructions: Case study using the Steig et al. (2009) antarctic temperature reconstruction. *J. Climate* **24**, 2099–2115 (2010).
7. D. P. Schneider, C. Deser, Y. Okumura, An assessment and interpretation of the observed warming of west antarctica in the austral spring. *Climate Dynam.* **38**, 323–347 (2012).
8. J. A. Screen, I. Simmonds, Half-century air temperature change above antarctica: Observed trends and spatial reconstructions. *J. Geophys. Res.* **117**, D16108 (2012).
9. G. J. Marshall, Half-century seasonal relationships between the southern annular mode and antarctic temperatures. *Int. J. Climatol.* **27**, 373–383 (2007).
10. R. L. Fogt, J. Perlwitz, A. J. Monaghan, D. H. Bromwich, J. M. Jones, G. J. Marshall, Historical SAM variability. Part II: Twentieth-century variability and trends from reconstructions, observations, and the IPCC AR4 models. *J. Climate* **22**, 5346–5365 (2009).
11. Q. Ding, E. J. Steig, D. S. Battisti, M. Küttel, Winter warming in west antarctica caused by central tropical pacific warming. *Nat. Geosci.* **4**, 398–403 (2011).
12. J. P. Nicolas, D. H. Bromwich, New reconstruction of antarctic near-surface temperatures: Multidecadal trends and reliability of global reanalyses. *J. Climate* **27**, 8070–8093 (2014).
13. K. L. Smith, L. M. Polvani, Spatial patterns of recent antarctic surface temperature trends and the importance of natural variability: Lessons from multiple reconstructions and the CMIP5 models. *Climate Dynam.* **48**, 2653–2670 (2017).

14. D. W. J. Thompson, J. M. Wallace, The arctic oscillation signature in the wintertime geopotential height and temperature fields. *Geophys. Res. Lett.* **25**, 1297–1300 (1998).
15. D. T. Shindell, G. A. Schmidt, Southern hemisphere climate response to ozone changes and greenhouse gas increases. *Geophys. Res. Lett.* **31**, L18209 (2004).
16. X. Li, D. M. Holland, E. P. Gerber, C. Yoo, Impacts of the north and tropical atlantic ocean on the antarctic peninsula and sea ice. *Nature* **505**, 538–542 (2014).
17. D. Irving, I. Simmonds, A new method for identifying the pacific–South american pattern and its influence on regional climate variability. *J. Climate* **29**, 6109–6125 (2016).
18. J. Turner, T. Phillips, J. Scott Hosking, G. J. Marshall, A. Orr, The amundsen sea low. *Int. J. Climatol.* **33**, 1818–1829 (2013).
19. K. C. Mo, M. Ghil, Statistics and dynamics of persistent anomalies. *J. Atmos. Sci.* **44**, 877–902 (1987).
20. S. E. Close, A. C. Naveira Garabato, E. L. McDonagh, B. A. King, M. Biuw, L. Boehme, Control of mode and intermediate water mass properties in drake passage by the amundsen sea low. *J. Climate* **26**, 5102–5123 (2013).
21. G. R. Simpkins, L. M. Ciasto, M. H. England, Observed variations in multidecadal antarctic sea ice trends during 1979–2012. *Geophys. Res. Lett.* **40**, 3643–3648 (2013).
22. A. Jenkins, D. Shoosmith, P. Dutrieux, S. Jacobs, T. W. Kim, S. H. Lee, H. K. Ha, S. Stammerjohn, West antarctic ice sheet retreat in the amundsen sea driven by decadal oceanic variability. *Nat. Geosci.* **11**, 733–738 (2018).
23. N. A. Rayner, D. E. Parker, E. B. Horton, C. K. Folland, L. V. Alexander, D. P. Rowell, E. C. Kent, A. Kaplan, Global analyses of sea surface temperature, sea ice, and night marine air temperature since the late nineteenth century. *J. Geophys. Res.* **108**, 4407 (2003).
24. G. R. North, T. L. Bell, R. F. Cahalan, F. J. Moeng, Sampling errors in the estimation of empirical orthogonal functions. *Mon. Weather Rev.* **110**, 699–706 (1982).
25. D. P. Schneider, E. J. Steig, J. C. Comiso, Recent climate variability in antarctica from satellite-derived temperature data. *J. Climate* **17**, 1569–1583 (2004).
26. T. Fan, C. Deser, D. P. Schneider, Recent antarctic sea ice trends in the context of southern ocean surface climate variations since 1950. *Geophys. Res. Lett.* **41**, 2419–2426 (2014).
27. J. J. Kennedy, N. A. Rayner, R. O. Smith, D. E. Parker, M. Saunby, Reassessing biases and other uncertainties in sea surface temperature observations measured in situ since 1850: 1. Measurement and sampling uncertainties. *J. Geophys. Res.* **116**, D14103 (2011).
28. J. Turner, H. Lu, I. White, J. C. King, T. Phillips, J. S. Hosking, T. J. Bracegirdle, G. J. Marshall, R. Mulvaney, P. Deb, Absence of 21st century warming on antarctic peninsula consistent with natural variability. *Nature* **535**, 411–415 (2016).
29. M. N. Raphael, A zonal wave 3 index for the southern hemisphere. *Geophys. Res. Lett.* **31**, L23212 (2004).
30. D. Irving, I. Simmonds, A novel approach to diagnosing southern hemisphere planetary wave activity and its influence on regional climate variability. *J. Climate* **28**, 9041–9057 (2015).
31. G. J. Marshall, D. W. J. Thompson, The signatures of large-scale patterns of atmospheric variability in antarctic surface temperatures. *J. Geophys. Res. Atmos.* **121**, 3276–3289 (2016).
32. K. E. Taylor, R. J. Stouffer, G. A. Meehl, An overview of CMIP5 and the experiment design. *Bull. Am. Meteorol. Soc.* **93**, 485–498 (2012).
33. J. Lee, K. R. Sperber, P. J. Gleckler, C. J. W. Bonfils, K. E. Taylor, Quantifying the agreement between observed and simulated extratropical modes of interannual variability. *Climate Dynam.* **52**, 4057–4089 (2019).
34. B. Stenni, M. A. J. Curran, N. J. Abram, A. Orsi, S. Goursaud, V. Masson-Delmotte, R. Neukom, H. Goosse, D. Divine, T. van Ommen, E. J. Steig, D. A. Dixon, E. R. Thomas, N. A. N. Bertler, E. Isaksson, A. Ekaykin, M. Werner, M. Frezzotti, Antarctic climate variability on regional and continental scales over the last 2000 years. *Clim. Past* **13**, 1609–1634 (2017).
35. Z. Liu, B. L. Otto-Bliesner, F. He, E. C. Brady, R. Tomas, P. U. Clark, A. E. Carlson, J. Lynch-Stieglitz, W. Curry, E. Brook, D. Erickson, R. Jacob, J. Kutzbach, J. Cheng, Transient simulation of last deglaciation with a new mechanism for bolling-allerod warming. *Science* **325**, 310–314 (2009).
36. R. L. Fogt, A. J. Wovrosh, R. A. Langen, I. Simmonds, The characteristic variability and connection to the underlying synoptic activity of the amundsen-bellingshausen seas low. *J. Geophys. Res.* **117**, D07111 (2012).
37. K. J. E. Walsh, I. Simmonds, M. Collier, Sigma-coordinate calculation of topographically forced baroclinicity around antarctica. *Dyn. Atmos. Ocean.* **33**, 1–29 (2000).
38. J.-S. Kug, J.-H. Jeong, Y.-S. Jang, B.-M. Kim, C. K. Folland, S.-K. Min, S.-W. Son, Two distinct influences of arctic warming on cold winters over north america and east asia. *Nat. Geosci.* **8**, 759–762 (2015).
39. D. M. Smith, N. J. Dunstone, A. A. Scaife, E. K. Fiedler, D. Copsey, S. C. Hardiman, Atmospheric response to arctic and antarctic sea ice: The importance of ocean–Atmosphere coupling and the background state. *J. Climate* **30**, 4547–4565 (2017).
40. S. Kobayashi, Y. Ota, Y. Harada, A. Ebita, M. Moriya, H. Onoda, K. Onogi, H. Kamahori, C. Kobayashi, H. Endo, K. Miyaoka, K. Takahashi, The JRA-55 reanalysis: General specifications and basic characteristics. *J. Meteorol. Soc. Japan. Ser. II* **93**, 5–48 (2015).
41. H. Goosse, V. Brovkin, T. Fichefet, R. Haarsma, P. Huybrechts, J. Jongma, A. Mouchet, F. Selten, P.-Y. Barriat, J.-M. Campin, E. Deleersnijder, E. Driesschaert, H. Goelzer, I. Janssens, M.-F. Loutre, M. A. Morales Maqueda, T. Opsteegh, P.-P. Mathieu, G. Munhoven, E. J. Pettersson, H. Renssen, D. M. Roche, M. Schaeffer, B. Tartinville, A. Timmermann, S. L. Weber, Description of the earth system model of intermediate complexity LOVECLIM version 1.2. *Geosci. Model Dev.* **3**, 603–633 (2010).
42. G. A. Meehl, W. M. Washington, J. M. Arblaster, A. Hu, H. Teng, J. E. Kay, A. Gettelman, D. M. Lawrence, B. M. Sanderson, W. G. Strand, Climate change projections in CESM1(CAM5) compared to CCSM4. *J. Climate* **26**, 6287–6308 (2013).

Acknowledgments

Funding: S.-Y.J., J.-H.K., and S.-J.K. were supported by the project PE20070 of the Korea Polar Research Institute. J.C. and S.-I.A. were supported by the National Research Foundation of Korea (NRF) grant funded by the Korea government (MSIT) (NRF-2018R1A5A1024958). B.-M.K. was supported by the National Research Foundation of Korea (NRF) grant funded by the Korea government (MEST) (2019R1A2C1005460). **Author contributions:** S.-Y.J., J.-H.K., and S.-J.K. designed the research and wrote the majority of the manuscript. S.-Y.J., J.C., and J.-H.K. conducted the statistical analyses and prepared the figures. S.-Y.J. conducted the climate model experiments. All of the authors discussed the results and wrote the manuscript. **Competing interests:** The authors declare that they have no competing interests. **Data and material availability:** All data needed to evaluate the conclusions in the paper are present in the paper and/or the Supplementary Materials. Additional data related to this paper may be requested from the authors.

Submitted 16 August 2019
Accepted 14 April 2020
Published 12 June 2020
10.1126/sciadv.aaz1490

Citation: S.-Y. Jun, J.-H. Kim, J. Choi, S.-J. Kim, B.-M. Kim, S.-I. An, The internal origin of the west-east asymmetry of Antarctic climate change. *Sci. Adv.* **6**, eaaz1490 (2020).